Supplementary Information to the paper:

Crystal structure, fluorescence and nanostructuration studies of a novel Zn^{II} anthracene-based curcuminoid

Núria Aliaga-Alcalde[a], Laura Rodriguez[b], Marilena Ferbinteanu[c], Petra Höfer[d] and Thomas Weyhermüller[d]*

[a] ICREA (Institució Catalana de Recerca i Estudis Avançats) & Universitat de Barcelona, Facultat de Química, Martí i Franquès, 1-11, 08028 Barcelona, Spain. [b]Universitat de Barcelona, Facultat de Química, Martí i Franquès, 1-11, 08028 Barcelona, Spain. [c]University of Bucharest, Inorganic Chemistry Department, Dumbrava Rosie 23, Bucharest 020462, Romania. [d]Max-Planck Institut für Bioanorganische Chemie, P.O. Box 10 13 65, D-45413 Mülheim an der Ruhr, Germany.

List of contents:

Figure S5. Cyclic voltammograms of the reduction processes of complex **2** (green) at a scan rate of 100 mV/s in distilled CH_2Cl_2 with 0.1 M $(NBu^n_4)PF_6$ as electrolyte. Potential values referred to Fc/Fc^+.

Figure S6. Cyclic voltammograms of the oxidation processes of complex **2** (green) at a scan rate of 100 mV/s in distilled CH_2Cl_2 with 0.1 M $(NBu^n_4)PF_6$ as electrolyte. Potential values referred to Fc/Fc^+.

Figure S7. Cyclic voltammograms (orange, CV) and differential Pulse voltammogram (red, DPV) of the quasi-reversible reduction processes of complex **1** at a scan rate of 1000 mV/s in distilled CH_2Cl_2 with 0.1 M $(NBu^n_4)PF_6$ as electrolyte. Potential values referred to Fc/Fc^+.

Figure S8. Normalized excitation spectrum of 9Accm in $1\cdot10^{-5}$M dichloromethane solution (λ_{em} = 575 nm).

Figure S9. Normalized excitation spectrum of **1** in $1\cdot10^{-5}$M dichloromethane solution (λ_{em} = 575 nm).

Figure S10. Normalized excitation spectrum of **2** in $1\cdot10^{-5}$M dichloromethane solution (λ_{em} = 575 nm).

Figure S11. AFM image of molecules of **1** on a graphite surface by dip-coating (500×500 nm); the graphite surface was immersed for few seconds in a solution of **1** in CH_2Cl_2 ($1.35\cdot10^{-5}$M) and analysis of the height.

Figure S12. Measure of the size (different lengths) of one molecule of **1**.

Figure S13. Additional pictures using confocal spectroscopy.

Molecular Orbital Diagrams from ADF calculations.

Figure S14. The MO diagram for the $[Cu(9Accm)_2(py)]$ complex (in SP geometry and C_{2v} symmetry) and the constituting fragments (metal ion and ligands). The red lines connect fragment orbitals with MOs containing them as major components. The lines in the left side between the *d* set and the complex identify the MOs assignable to the Ligand Field scheme.

Figure S15. The MO diagram for the $[Zn(9Accm)_2(py)]$ complex (in TBP geometry and C_2 symmetry) and the constituting fragments (metal ion and ligands). The absence of the lines between the *d* set and the complex MOs is due to the fact that the metal ion AOs are smeared in relatively small portions over many doubly occupied MOs, as expression of ionic character of the bonding.

MO components from ADF calculations assignable to Ligand Field Scheme

Figures S16-1 to S16-5.

(Together with additional note)

Figure S17. The rationalization of the TD-DFT transitions that are assignable to the Ligand Field spectrum of d^9 configuration in $[Cu(9Accm)_2(py)]$ compound idealized to C_{2v}. The data correspond to Time Dependent (TD) unrestricted DFT calculation with the B3LYP functional. The density difference map figured in the upper part can be assigned to *d-d* electron density displacement. The yellow area corresponds to the shape of the orbital from where the electron is moved and the blue one corresponds to its location after transition. In all the cases the blue area of density accumulation is placed in the equatorial plane, corresponding to the unpaired electron of the d^9 set. Note that the sign of the orbitals is not retrieved in the density difference maps. The difference is taken as the full density of the excited state minus the full density of the ground state.

(Additional table attached)

Frontier Molecular Orbitals from unrestricted B3LYP calculations.

Figure S18. The frontier MOs for the C_{2v} idealized $[Cu(9Accm)_2(py)]$ from unrestricted DFT calculation with the B3LYP functional. The orbital assignable to the unpaired electron on the Cu^{II} ion, combined with in plane donor functions is placed at the position α 281. In principle, in the unrestricted frame, the α and β orbital sets are independent, but except the supplementary *d*-type MO there is a good resemblance between couples of spinorbitals, such as α_i is almost the same with β_{i-1} for labels i >281 and $\alpha_i \cong \beta_i$ for i < 281 lower orbitals.

(Table attached)

Spin density in ground and excited states of the Cu(II) complex.

Figure S19. (a) Spin density in the groundstate of C_{2v} idealized $[Cu(9Accm)_2(py)]$ and (b) an excited state with spin polarized nature (obtained by Broken Symmetry DFT) located at about 20000 cm^{-1}. The surfaces are drawn at 0.0015 e/$Å^3$. The α spin density is marked in blue, the β zones in green. In groundstate the total S_z= +1/2 projection is cumulated in the coordination equatorial plane. In the excited state the equatorial plane carries a S_z= -1/2 spin density, while the ligand part a triplet-like one, S_z= +1 (the total spin projection being S_z= 1/2).

(Additional Note)

Density Difference Maps for TD-DFT states.

Figure S20. The density difference maps for TD-DFT states of the idealized $[Zn(9Accm)_2(py)]$ complex with C_{2v} symmetry. View along the C_2 axis. The representation corresponds to the total density of excited state minus the density at the

groundstate. The blue areas represent the zones where the density moves during the transiton, the yellow ones corresponding to density depletion. All the cases correspond to $^1A_1 \rightarrow {}^1B_2$ transitions. The (a) diagram corresponding to the 13-th state and (b) to the 40-st one, in the series of computed TD-DFT levels. The wavelength (λ) and relative intensity (*f*) are marked near each panel.

(Additional Note)

Figure S21. The density difference map for the selected most intense transitions in the TD-DFT spectrum of the [Cu(9Accm)$_2$(py)] experimental structure (compound 2). The states libelled with their order numbers, their energies and computed intensity (*f*) are given below each inset. The blue areas represent the zones where the density moves during the transiton, the yellow ones corresponding to density depletion.

(Additional Note)

Figure S22. The density difference map for the [Zn(9Accm)$_2$(py)] experimental structure (compound **1**).

(Additional Note)

Table S1. Comparison of the crystallographic data and collection parameters of complexes **1** and **2**.

	1	**2**
Formula	$C_{75}H_{51}NO_4Zn$	$C_{75}H_{51}CuNO_4$
FW	1095.54	1093.72
Space group	*C2*	*P* ī
***a*/Å**	23.545(16)	9.135(4)
***b*/Å**	8.979(6)	11.707(5)
***c*/Å**	13.021(9)	25.643(9)
α/deg.	90.00	86.746(8)
ß/deg.	91.567(15)	85.276(9)
γ/deg.	90.00	81.373(9)
***V*/ Å^3**	2752(3)	2699.4(19)
Z	2	2
***T*, K**	100(2)	100
λ(MoK$_\alpha$) Å	0.71073	0.71073
ρ_{calc}, Mg·cm^{-3}	1.322	1.346
μ(MoK$_\alpha$) mm^{-1}	0.502	0.461
***R*1 [$I > 2\sigma(I)$]**	0.0638	0.0428
ωR2 (all data)	0.1284	0.1077

Table S2. Selected interatomic distances (Å) and angles (deg) for compound **1**.

Zn(1)-O(19)	1.977(4)	**O(19)#-Zn(1)-O(17)#**	89.67(18)
Zn(1)-O(19)#	1.977(4)	**O(17)-Zn(1)-O(17)#**	175.3(3)
Zn(1)-O(17)	2.041(4)	**O(19)-Zn(1)-N(41)**	126.06(13)
Zn(1)-O(17)#	2.041(4)	**O(19)#-Zn(1)-N(41)**	126.06(13)
Zn(1)-N(41)	2.123(8)	**O(17)#-Zn(1)-N(41)**	87.65(17)
O(17)-C(17)	1.263(7)	**O(17)-Zn(1)-N(41)**	87.65(17)
C(17)-C(18)	1.389(9)	**C(17)-O(17)-Zn(1)**	125.4(4)
C(18)-C(19)	1.387(9)	**O(17)-C(17)-C(18)**	124.0(6)
O(19)-C(19)	1.292(7)	**C(19)-C(18)-C(17)**	126.7(6)
O(19)-Zn(1)-(O19)#	107.9(3)	**C(19)-O(18)-H(18)**	116.7
O(19)-Zn(1)-(O17)	89.67(18)	**C(17)-C(18)-H(18)**	116.7
O(19)#-Zn(1)-(O17)	93.10(18)	**C(19)-O(19)-Zn(1)**	127.1(4)
O(19)-Zn(1)-(O17)#	93.10(18)	**O(19)-C(19)-C(18)**	124.4(6)

Table S3. Comparison of the selected interatomic distances (Å) and angles (deg) of complexes **1** and **2**.

Zn(1)-O(19)	1.977(4)	**O(19)#-Zn(1)-O(17)#**	89.67(18)
Zn(1)-O(19)#	1.977(4)	**O(17)-Zn(1)-O(17)#**	175.3(3)
Zn(1)-O(17)	2.041(4)	**O(19)-Zn(1)-N(41)**	126.06(13)
Zn(1)-O(17)#	2.041(4)	**O(19)#-Zn(1)-N(41)**	126.06(13)
Zn(1)-N(41)	2.123(8)	**O(17)#-Zn(1)-N(41)**	87.65(17)
O(17)-C(17)	1.263(7)	**O(17)-Zn(1)-N(41)**	87.65(17)
C(17)-C(18)	1.389(9)	**C(17)-O(17)-Zn(1)**	125.4(4)
C(18)-C(19)	1.387(9)	**O(17)-C(17)-C(18)**	124.0(6)
O(19)-C(19)	1.292(7)	**C(19)-C(18)-C(17)**	126.7(6)
O(19)-Zn(1)-(O19)#	107.9(3)	**C(19)-O(18)-H(18)**	116.7
O(19)-Zn(1)-(O17)	89.67(18)	**C(17)-C(18)-H(18)**	116.7
O(19)#-Zn(1)-(O17)	93.10(18)	**C(19)-O(19)-Zn(1)**	127.1(4)
O(19)-Zn(1)-(O17)#	93.10(18)	**O(19)-C(19)-C(18)**	124.4(6)
Cu(1)-O(19)	1.924(2)	**O(57)-Cu(1)-O(59)**	92.48(10)
Cu(1)-O(57)	1.928(2)	**O(17)-Cu(1)-O(59)**	88.08(10)
Cu(1)-O(17)	1.932(2)	**O(19)-Cu(1)-N(81)**	109.54(11)
Cu(1)-O(59)	1.943(2)	**O(57)-Cu(1)-N(81)**	98.73(10)
Cu(1)-N(81)	2.331(3)	**O(17)-Cu(1)-N(81)**	89.44(10)
O(17)-C(17)	1.272(4)	**O(59)-Cu(1)-N(81)**	84.38(10)
O(19)-C(19)	1.279(4)	**C(17)-O(17)-Cu(1)**	126.0(2)
O(57)-C(57)	1.285(4)	**O(17)-C(17)-C(18)**	124.6(3)
O(59)-C(59)	1.283(4)	**O(19)-C(19)-C(18)**	123.9(3)
O(19)-Cu(1)-O57	85.07(10)	**C(57)-O(57)-Cu(1)**	124.6(2)
O(19)-Cu(1)-O17	92.43(10)	**O(57)-C(57)-C(58)**	124.7(3)
O(57)-Cu(1)-O17	171.83(11)	**C(59)-O(59)-Cu(1)**	121.9(2)
O(19)-Cu(1)-O59	166.07(11)	**O(59)-C(59)-C(58)**	124.7(3)

Figure S1

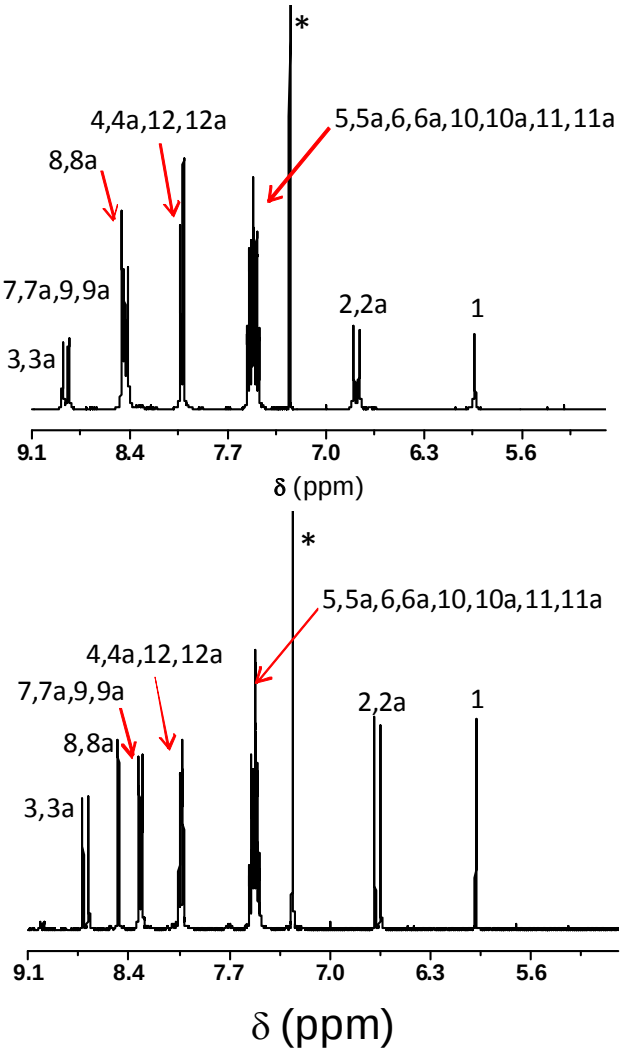

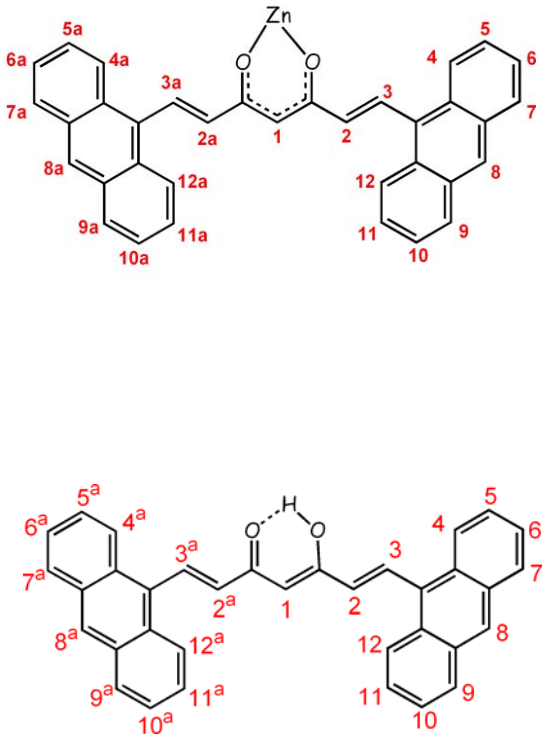

Protons labeled 2, 2a, 3, 3a, 7, 7a, 9 and 9a are ca. 0.15 ppm downfield shifted with respect to the free 9accm ligand.

Figure S2

(a)

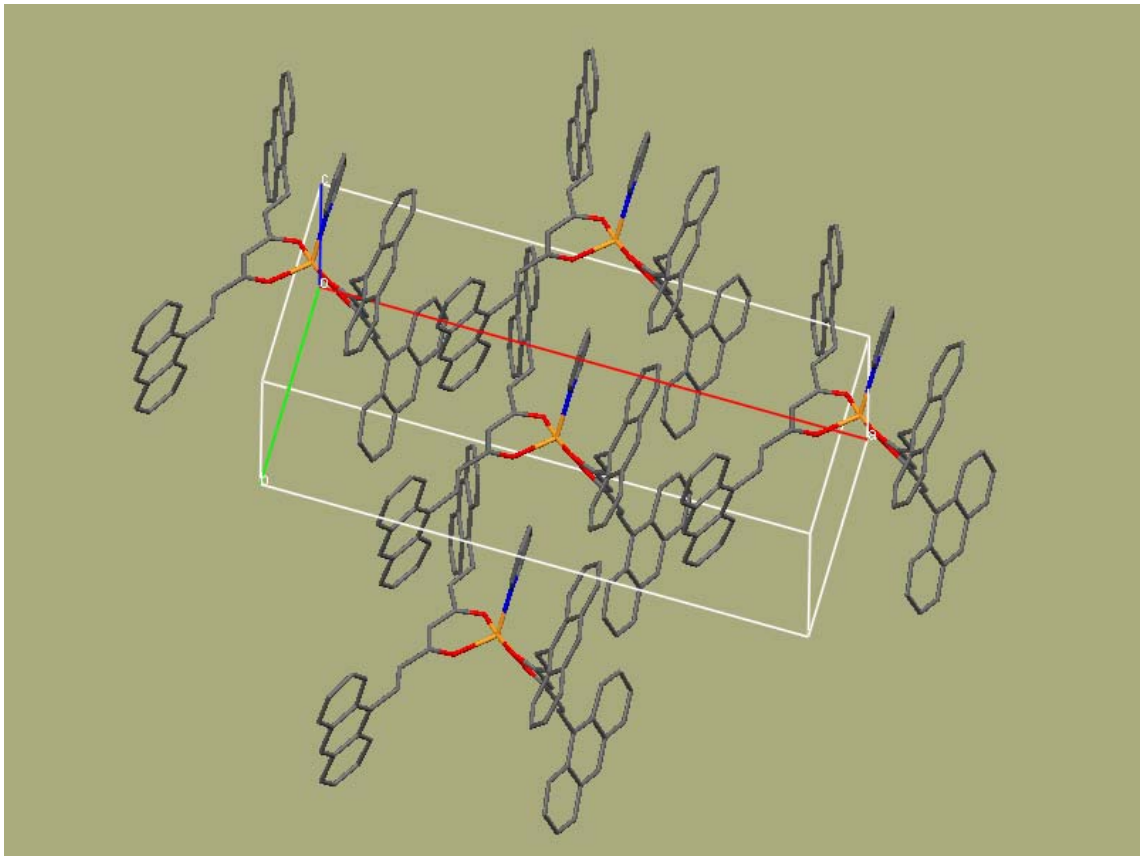

Figure S2

(b)

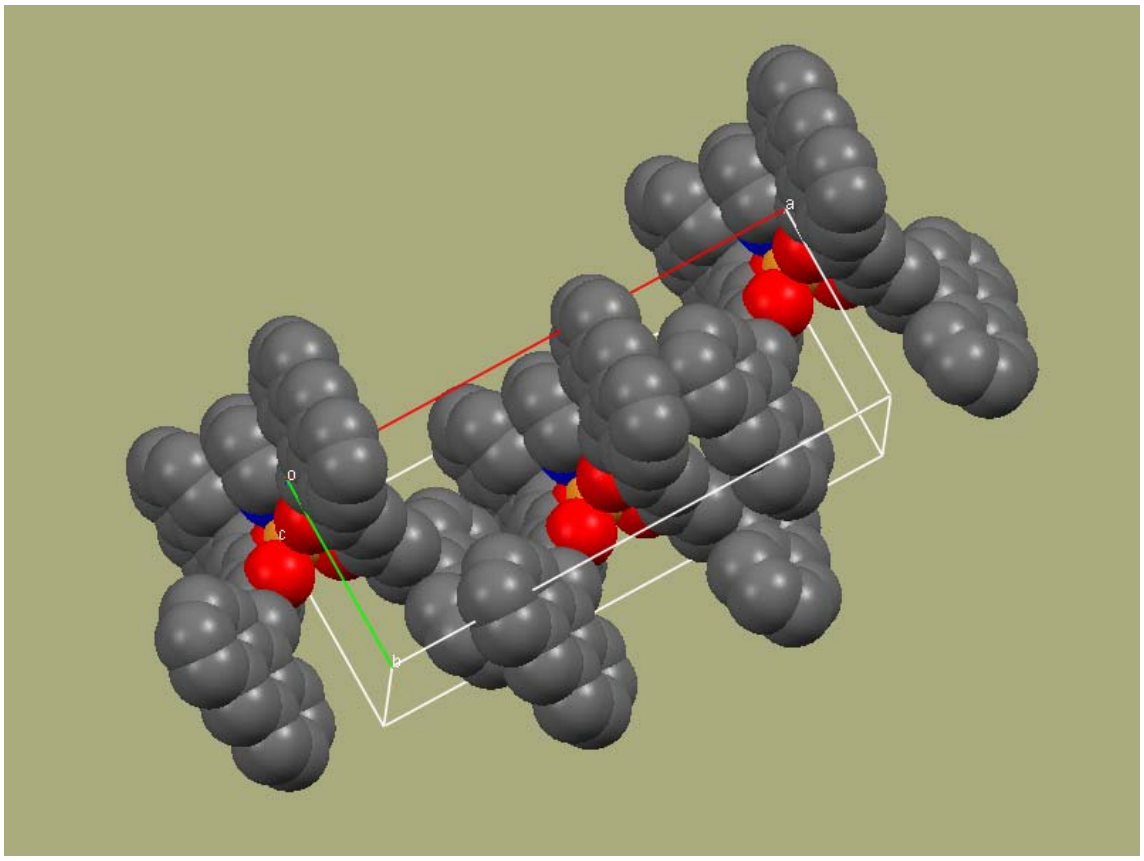

Figure S3

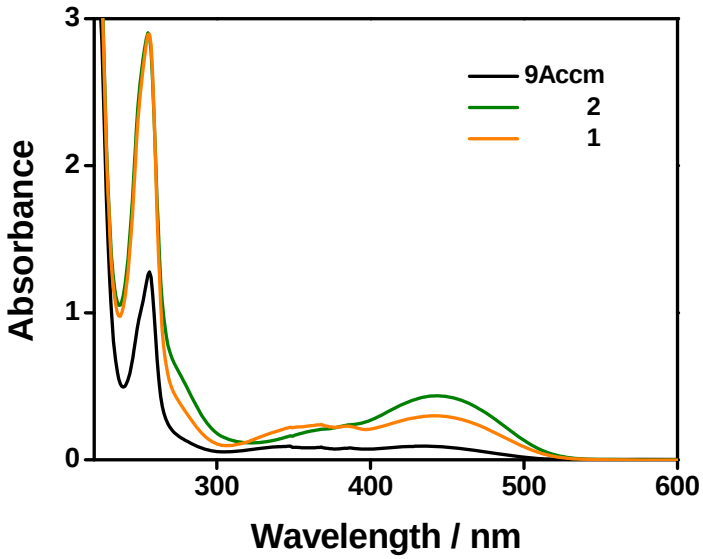

Figure S4

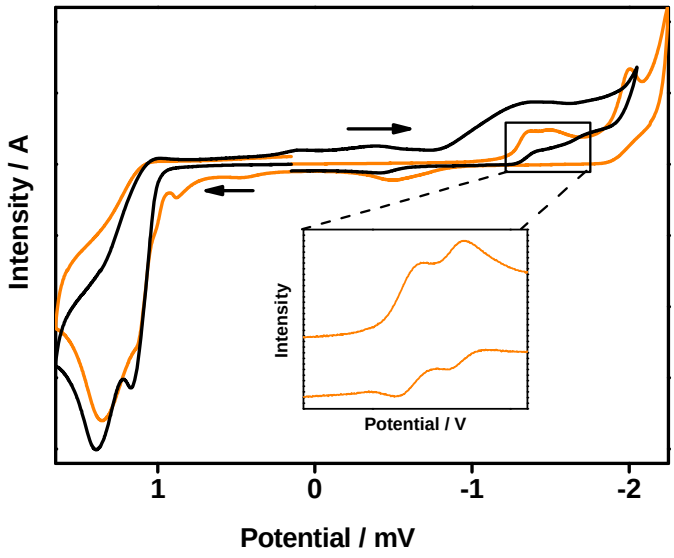

Figure S5

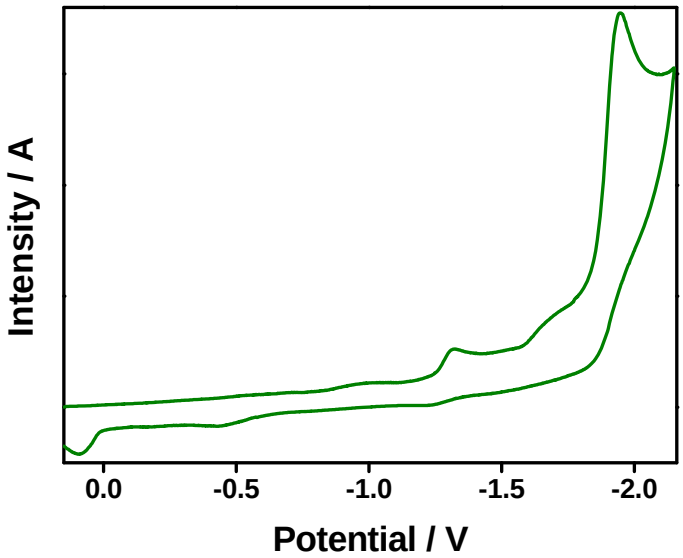

Figure S6

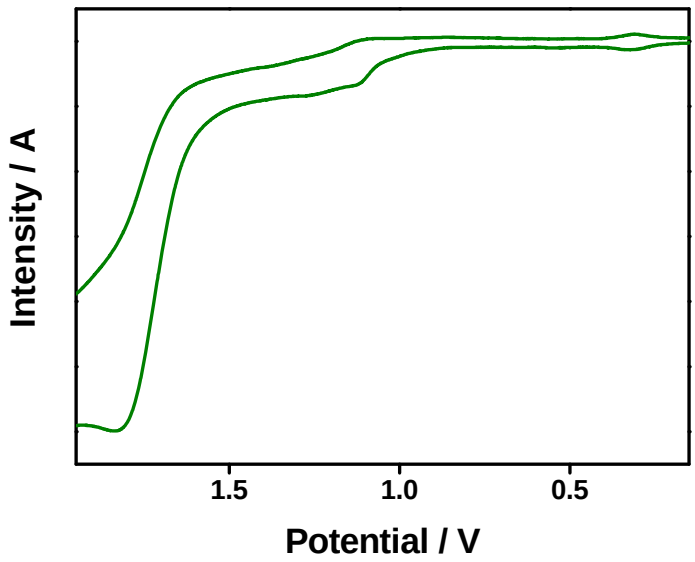

Figure S7

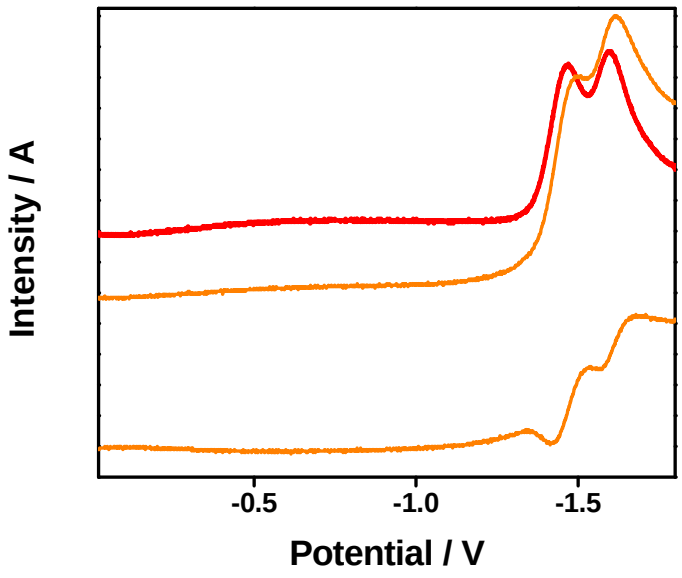

Figure S8

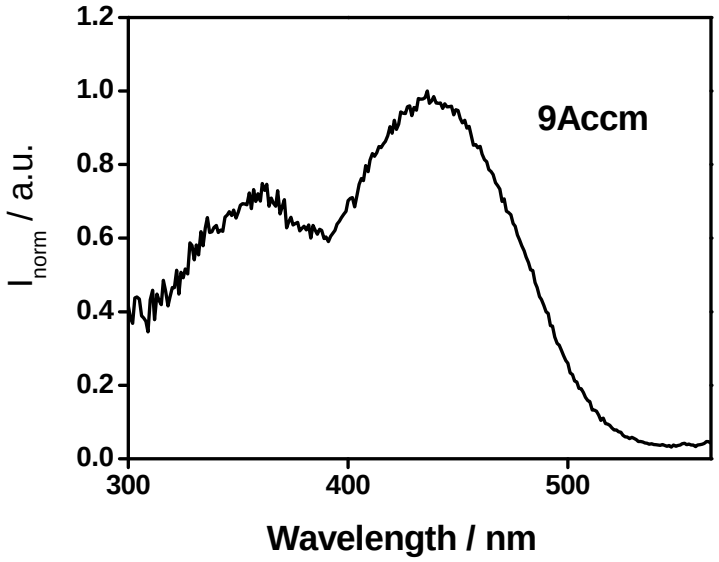

Figure S9

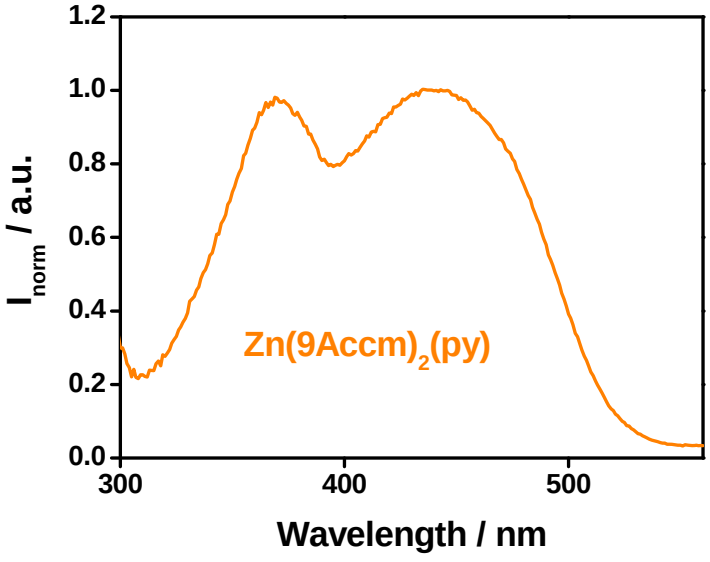

Figure S10

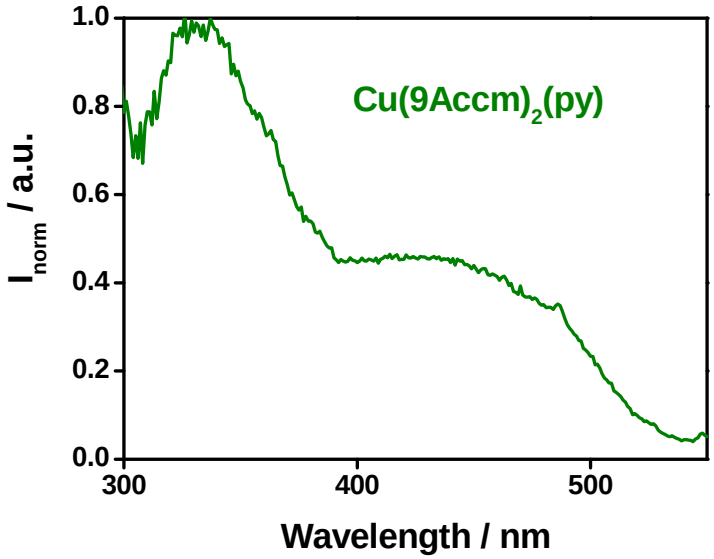
1.0
0.8
0.6
0.4
0.2
0.0
300
400
500
I_{norm} / a.u.
Wavelength / nm
Cu(9Accm)$_2$(py)

Figure S11

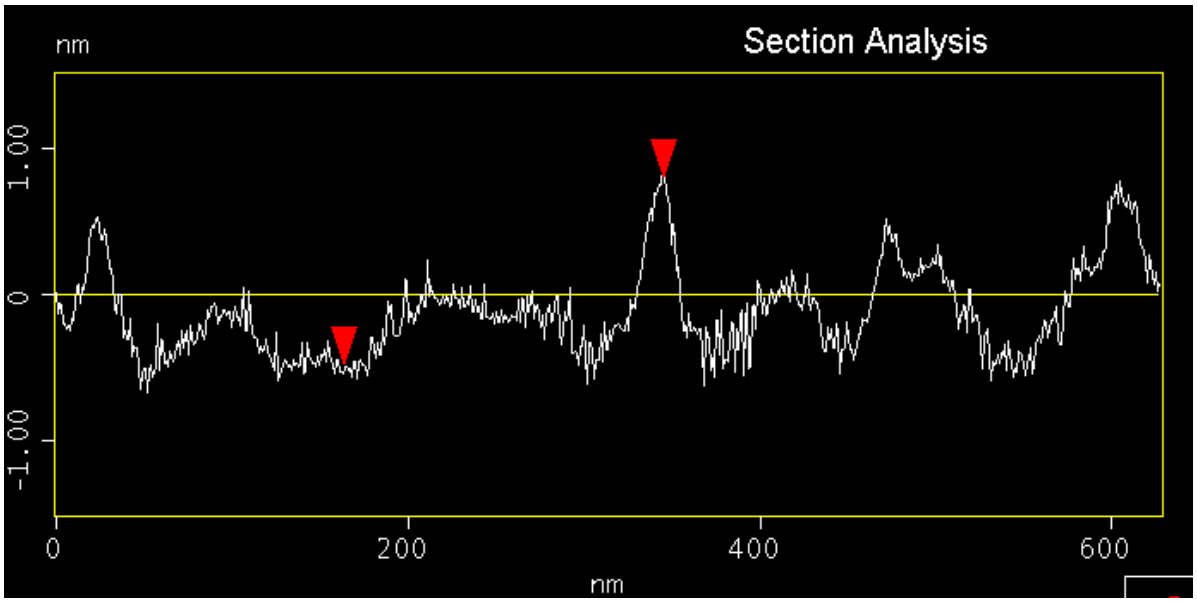

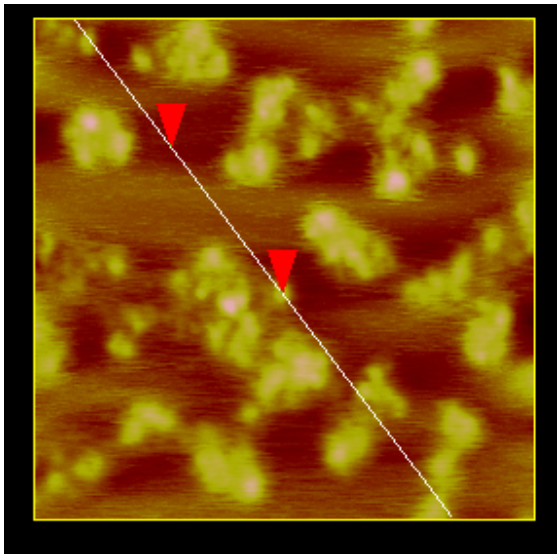

Surface distance	182.75 nm
Horiz distance(L)	181.64 nm
Vert distance	1.279 nm
Angle	0.403 °
Surface distance	
Horiz distance	
Vert distance	
Angle	
Surface distance	
Horiz distance	
Vert distance	
Angle	
Spectral period	DC
Spectral freq	0 /nm
Spectral RMS amp	0.161 nm

Figure S12

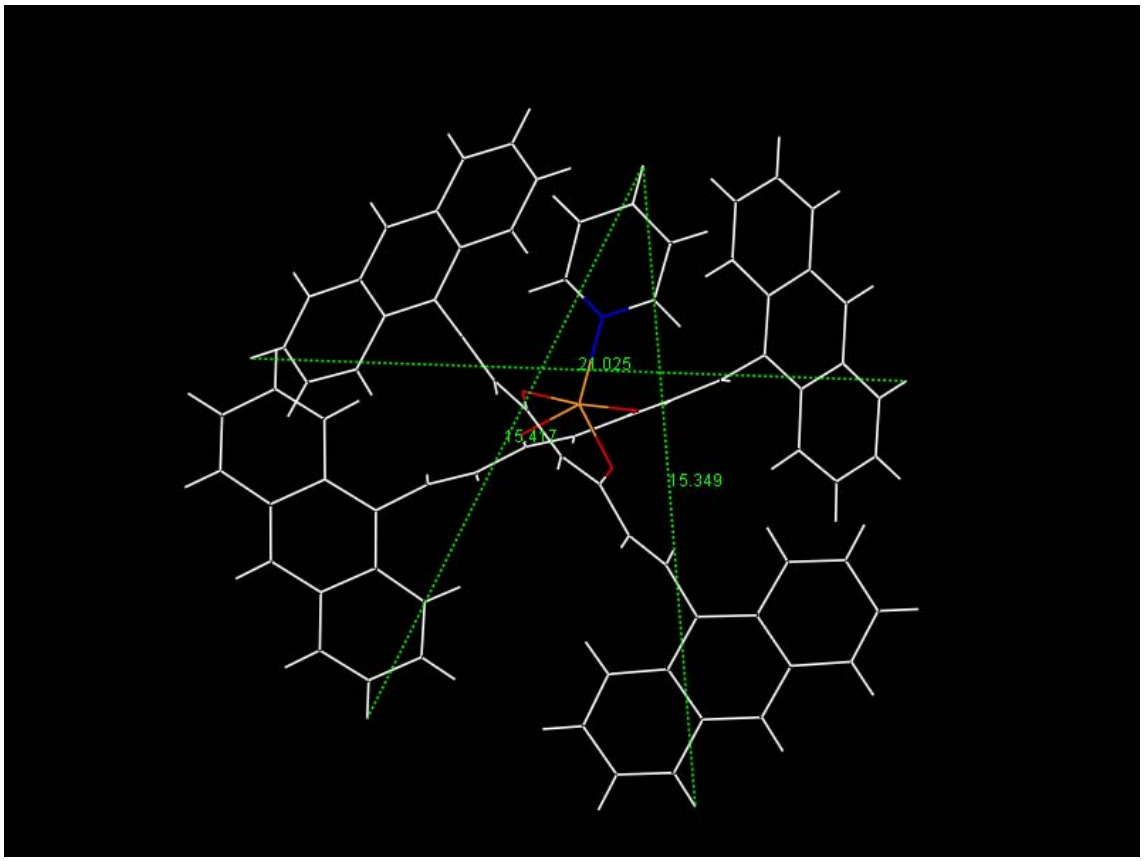

Figure S13

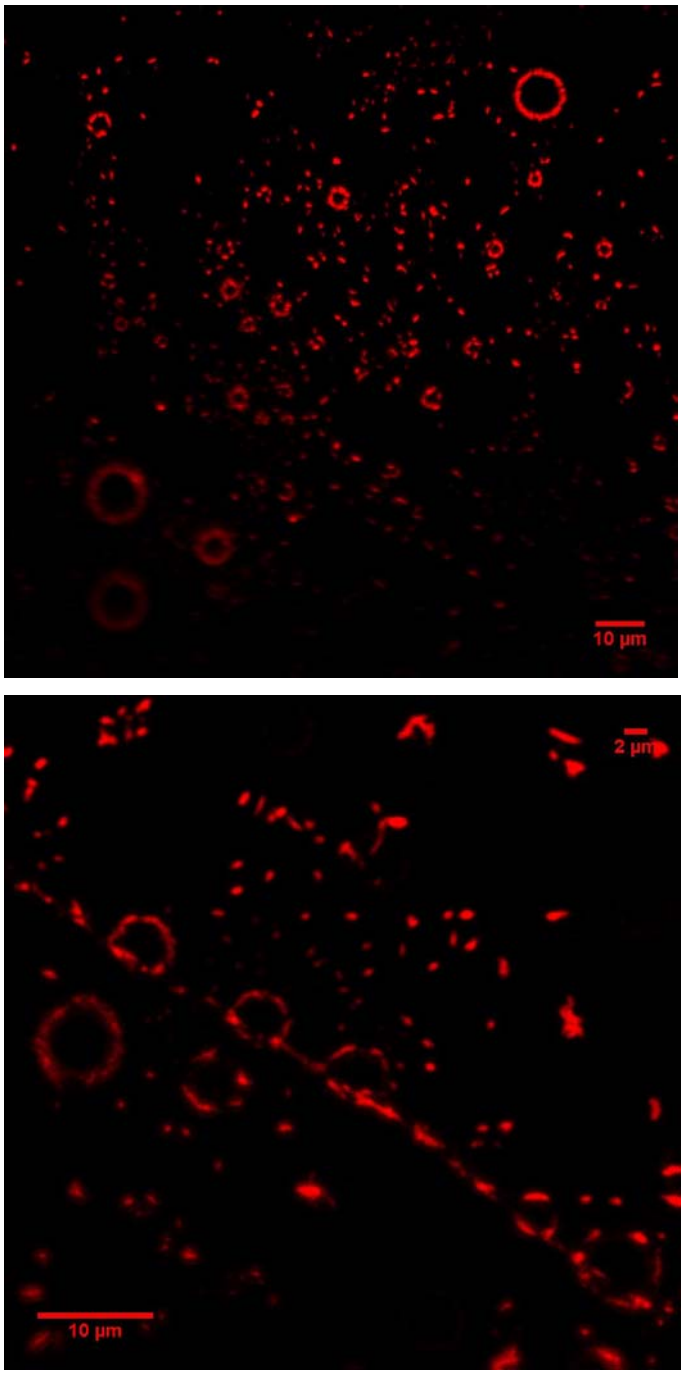

Molecular Orbital Diagrams from ADF calculations.

Figure S14

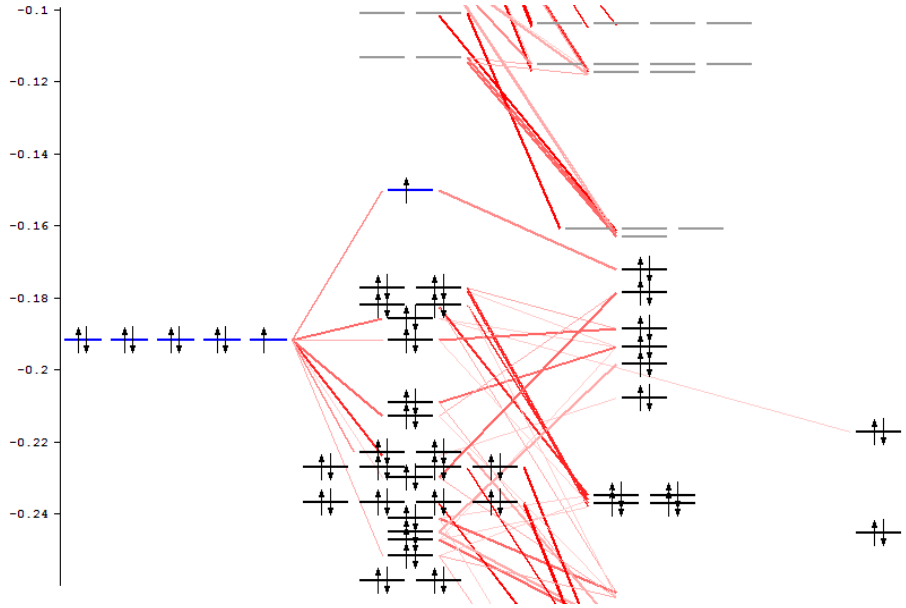

Cu(II) [Cu(9Accm)$_2$Py] 2 × (9Accm$^-$) Py

Figure S15

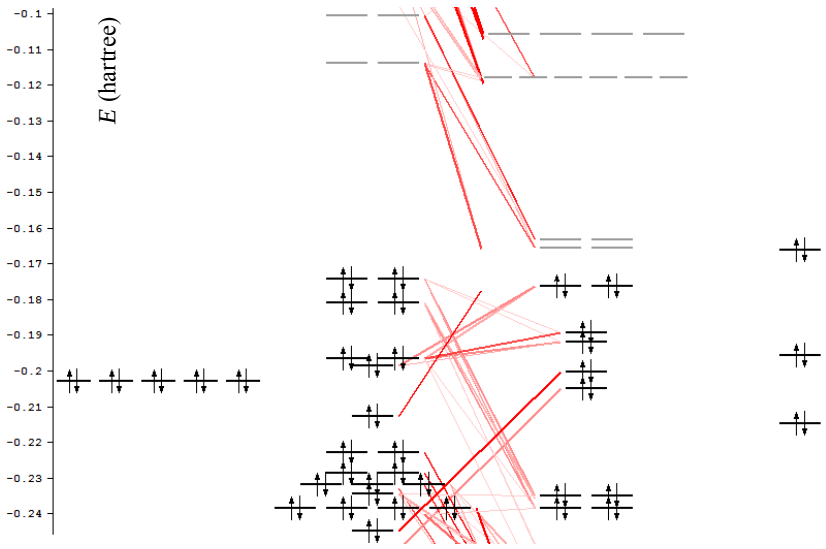

Zn(II) [Zn(9Accm)$_2$Py] 2 × (9Accm$^-$) Py

MO components from ADF calculations assignable to Ligand Field Scheme

==========

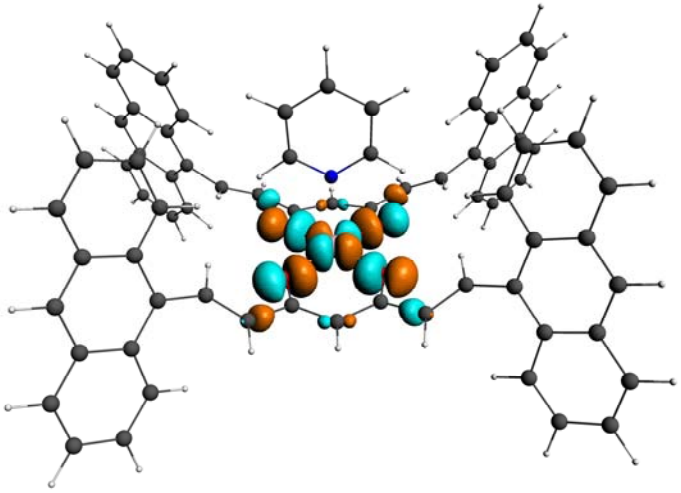

Fig. S16-1

E(eV)	Occ	MO	%	Fragment MO	Fragment
-4.087	1	63 A2	47.24%	*xy*	M
			45.79%	61 A2	$(9Accm^-)_2$
			2.47%	62 A2	$(9Accm^-)_2$

==========

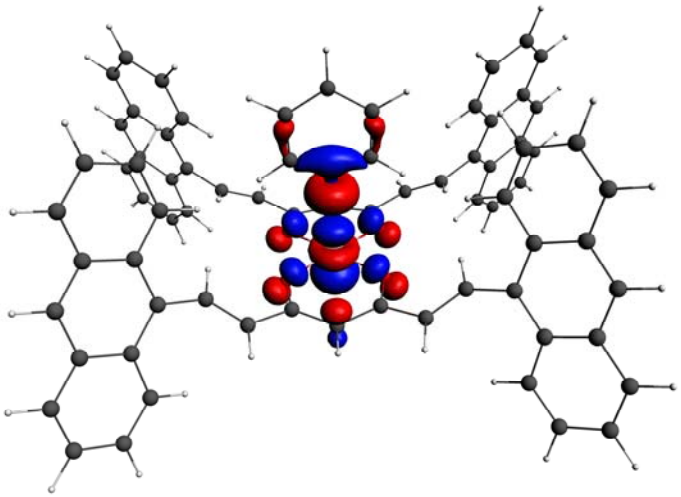

Fig. S16-2

E(eV)	Occ	MO	%	Fragment MO	Fragment
-5.058	2	81 A1	52.66%	z^2	M
			19.48%	11 A1	py
			11.94%	64 A1	$(9Accm^-)_2$
			9.79%	63 A1	$(9Accm^-)_2$
			2.15%	62 A1	$(9Accm^-)_2$

==========
=

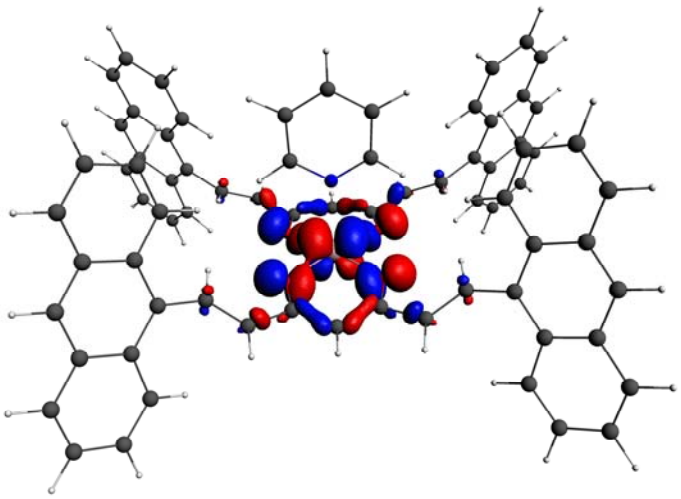

Fig. S16-3

E(eV)	Occ	MO	%	Fragment MO	Fragment
-5.795	2	70 B2	52.29%	*xz*	M
			29.96%	61 B2	$(9Accm^-)_2$
			11.79%	59 B2	$(9Accm^-)_2$
			2.69%	60 B2	$(9Accm^-)_2$
			1.69%	62 B2	$(9Accm^-)_2$

==========
=

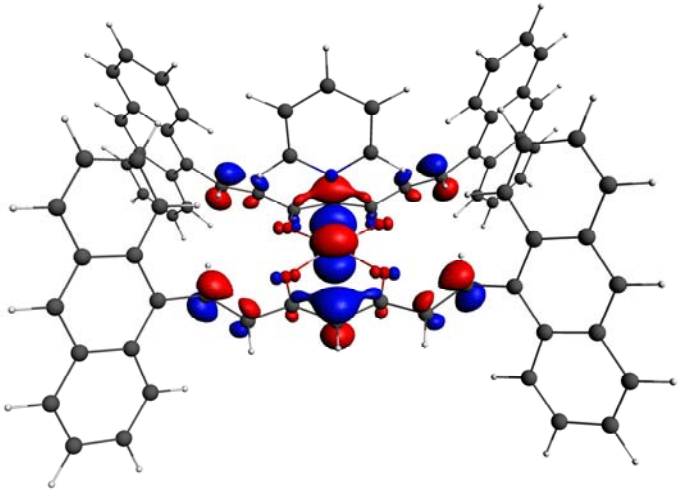

Fig. S16-4

E(eV)	Occ	MO	%	Fragment MO	Fragment
-6.065	2	67 B1	46.74%	*yz*	M
			36.75%	61 B1	$(9Accm^-)_2$
			9.15%	64 B1	$(9Accm^-)_2$
			4.43%	63 B1	$(9Accm^-)_2$

==========
=

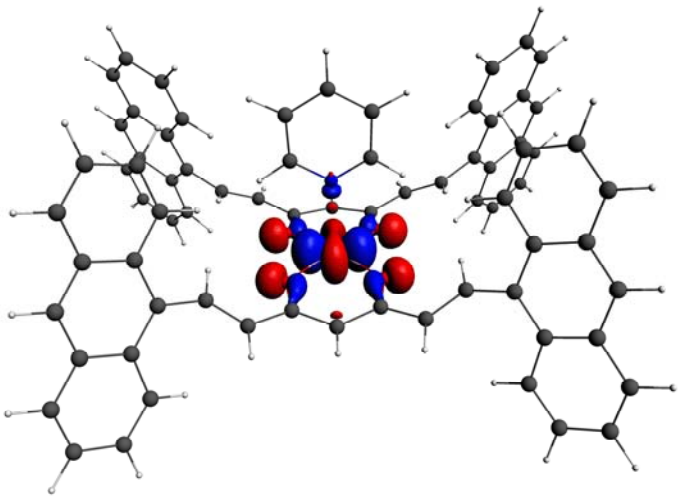

Fig. S16-5

E(eV)	Occ	MO	%	Fragment MO	Fragment
-6.093	2	79 A1	73.96%	x^2-y^2	M
			13.22%	63 A1	2´(9Accm)
			4.87%	z^2	M
			3.14%	58 A1	2´(9Accm)

==========
=

Note that due to conventional axis choice specific to C_{2v} point group the *d* orbital label differ from standard denomination with respect of octahedral parentage. Because the x and y are pointing toward edges of the equatorial plane (not to vertices, as in textbook Ligand Field diagrams) the xy and x^2-y^2 components are mutually switched. Thus, in the actual case the highest Ligand Field type MO, the carrier of unpaired electron is an a_2 function preponderantly made of *xy*. In formal O_h reference this component is equivalent to the x^2-y^2.

The actual orbital ordering is $a_1 < b_1 < b_2 < a_1 < a_2$, which converted to the conventional notation of LF orbitals reads as follows: $xy < xz < yz < z^2 < x^2$-y^2.

The above MO pictures are given in the order of decreasing energy, the first MO picture corresponding to the carrier of the unpaired electron.

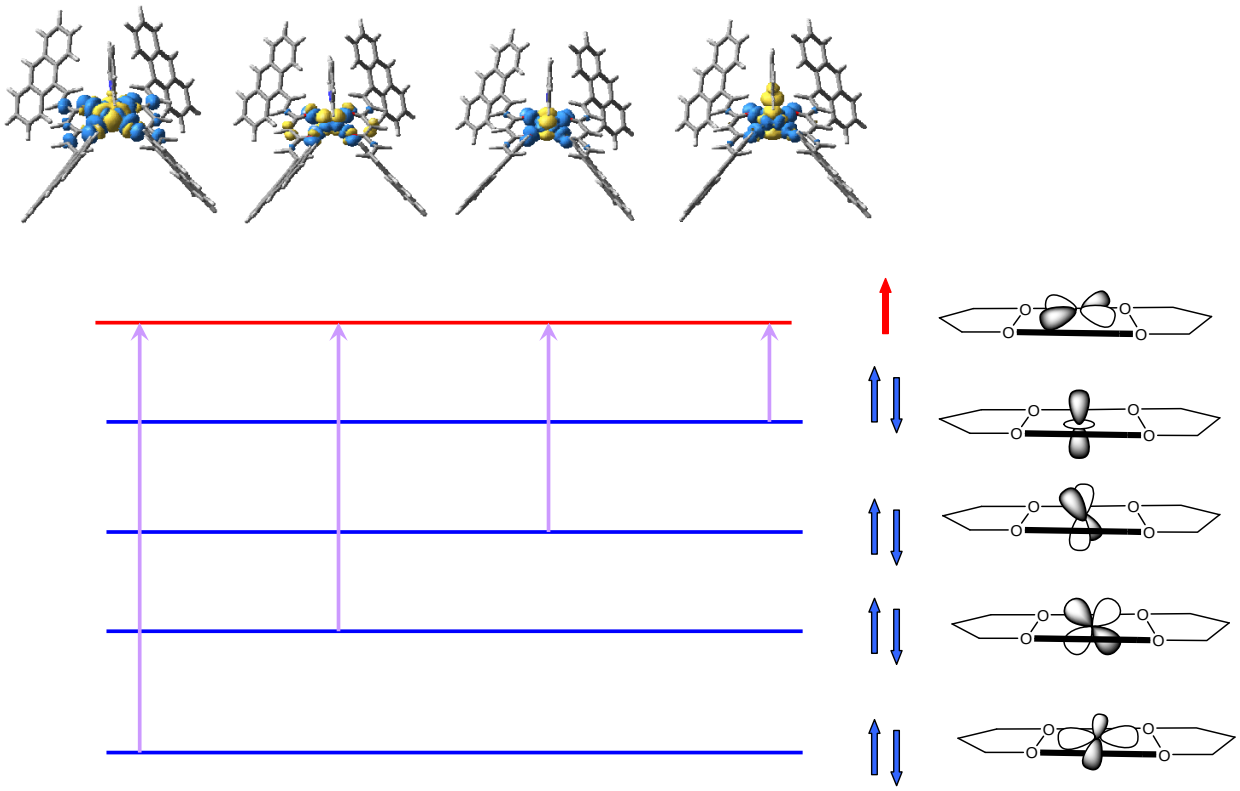

Figure S17.

Assignment, energy and wavelength of the TD-DFT excitations identified as Ligand Field type transitions.

TD transition no.	Assignment	*E*(cm)	λ(nm)
1	$^2A_2 \rightarrow {}^2A_2$	10810.7	925.0
7	$^2A_2 \rightarrow {}^2B_2$	13487.1	741.5
8	$^2A_2 \rightarrow {}^2B_1$	15585.1	641.6
9	$^2A_2 \rightarrow {}^2A_2$	16401.0	609.7

Frontier Molecular Orbitals from unrestricted B3LYP calculations.

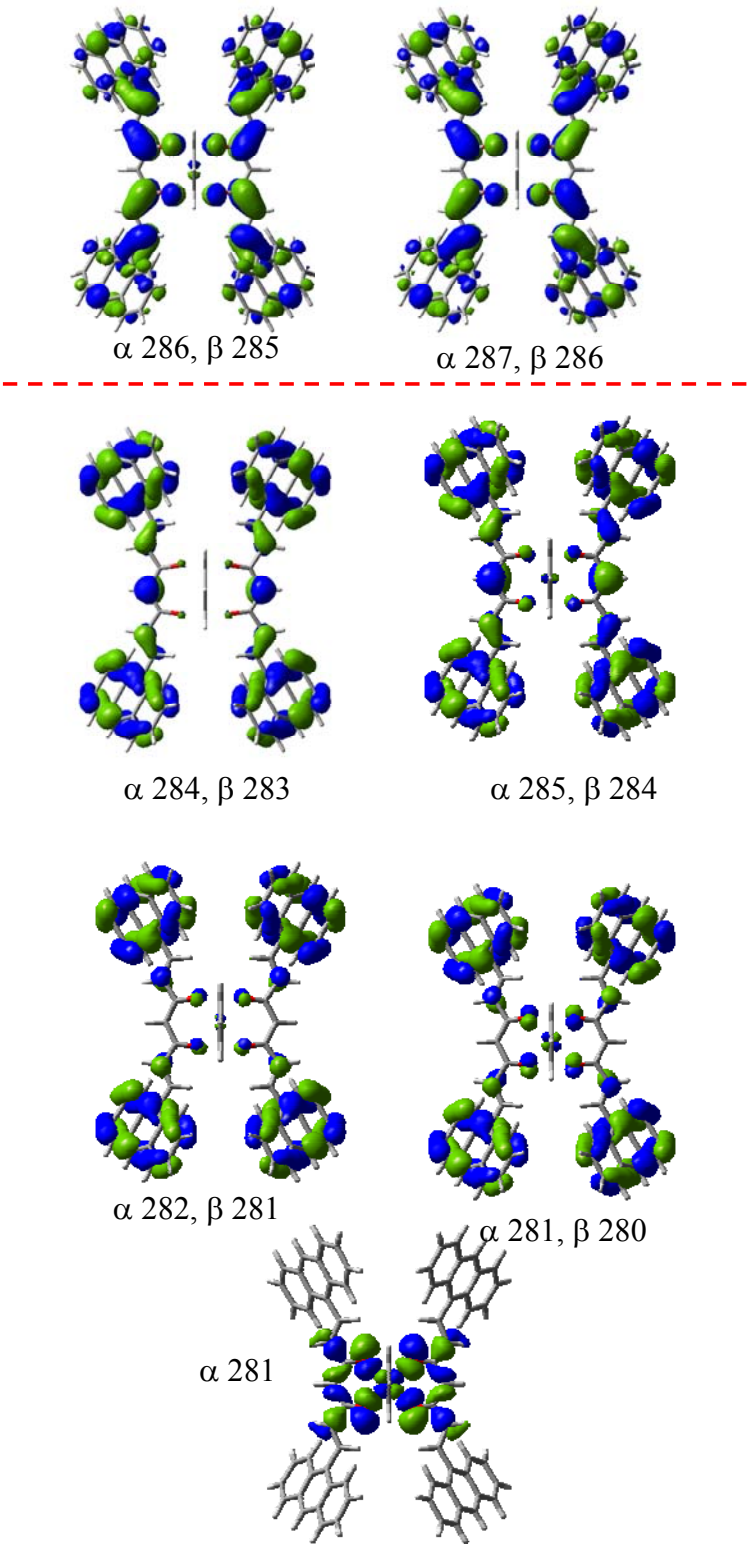

Figure S18.

The orbital promotions for the excited states discussed in main text and represented in Figure M1 are as follows:

Excited State 13
(λ=483.75 nm, *f*=1.20 a.u.)

Orbital promotion	Coefficient
α 284 → α 286	0.60060
α 285 → α 287	0.35029
β 283 → β 285	0.45565
β 284 → β 286	0.44539

Excited State 40
(λ=399.5 nm, *f*=0.16 a.u.)

Orbital promotion	Coefficient
α 280 → α 287	0.59666
α 282 → α 288	-0.36283
α 283 → α 289	-0.17979
β 278 → β 285	-0.13722
β 279 → β 285	-0.16167
β 280 → β 286	0.49532
β 281 → β 287	-0.25145
β 283 → β 289	0.16289

Spin density in ground and excited states of the Cu(II) complex.

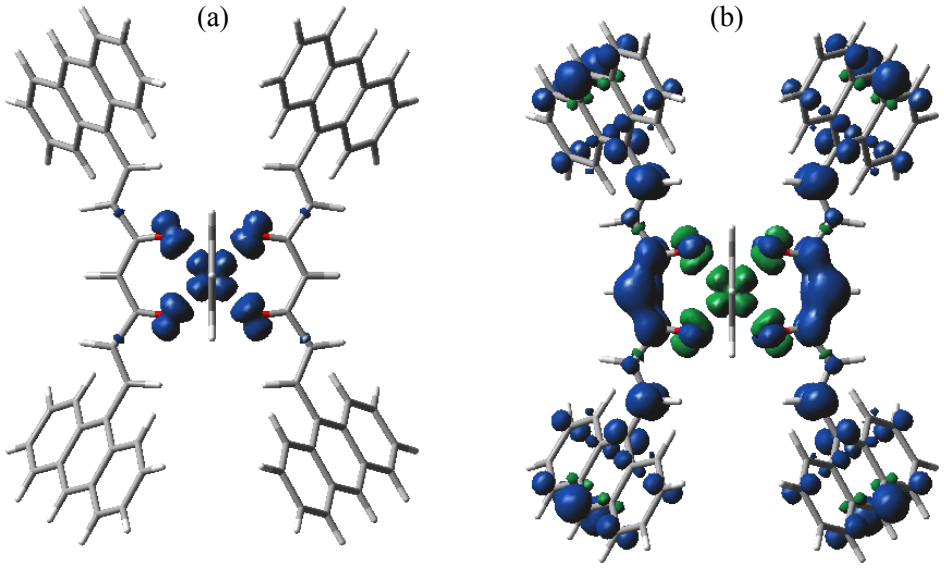

Figure S19.

Both states in Figure S17 have the same total spin projection (doublet type). The fact that the excited state is located nearby the TD-DFT state with the high intensity (see the text) responsible for absorption and potential luminiscence effects, supports the point that the spin coupling induces an enhanced configuration interaction coupling between the states of Cu(II) complex (in comparison to the Zn(II) hypothetic similar structure). This determines a possibility for non-radiative de excitation and the quenching of luminiscence. In order to get explicit spin density we used a Broken Symmetry DFT approach. [1,2]

[1] (a) Noodleman L, Norman JG (1979) J. Chem. Phys. 70: 4903; (b) Noodleman L (1981) J Chem Phys 74:5737. (c) L, Peng CY, Case DA, Mouesca JM (1995) Coord Chem Rev 144:199.

Density Difference Maps for TD-DFT states.

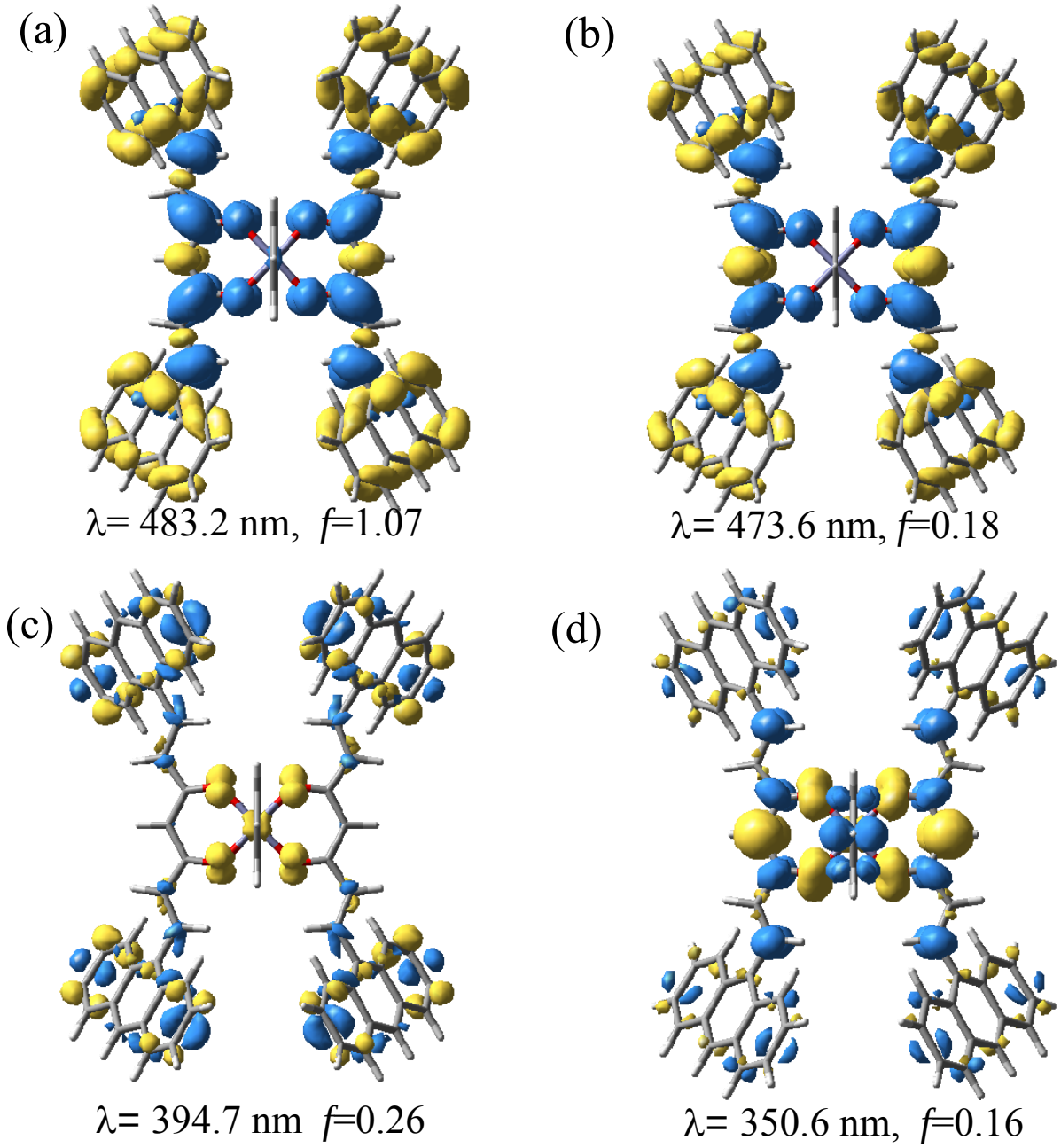

Figure S20.

---

[2] (a) Ruiz E (2004) Struct Bonding 113:71.(b) Ruiz E, Alemany P, Alvarez S, Cano J (1997) J Am Chem Soc 119:1297; Ruiz E, Cano J, Alvarez S, Alemany P, (1999) J Comput Chem 20:1391. (c) Daul CA, Ciofini I, Bencini A (2002) in Reviews of Modern Quantum Chemistry, part II (Ed.: K. D. Sen), World Scientific, Singapore, 1247.

In the following the density difference maps associated for the selected TD-DFT states computed at experimental structures of compound **1** and **2** will be presented.

For Cu(II) system, the first two intense transitions (#12 and #16) show like a transition from states located on anthracene fragments to the diketonate moieties of the ligands. There is a slight implication of the metal ion in this process. A higher intense transition #36 has the intriguing aspect of the intra-ligand charge transfer, namely between the two anthracene moieties.

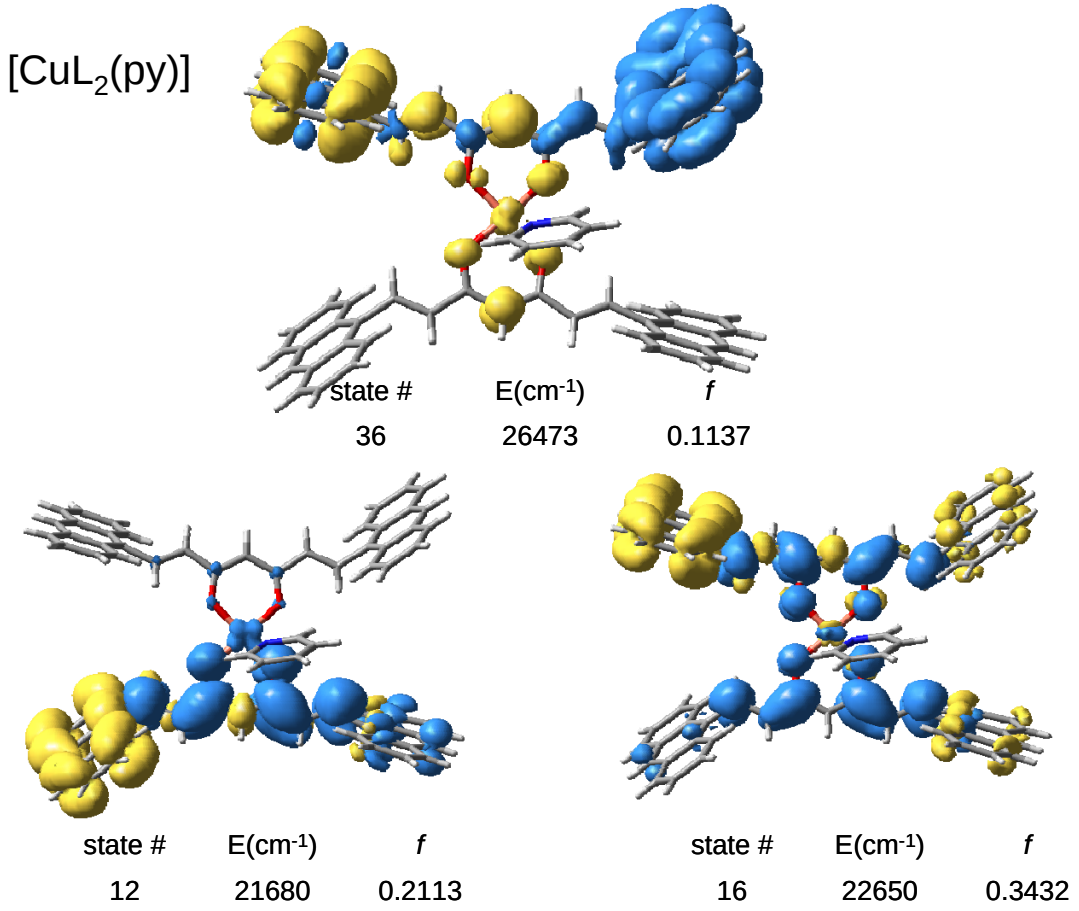

Figure S21.

The the Zn(II) system, the two intense bands (also the lowest excitations, #1 and #2) have both the aspect of a transition from anthracene aromatic part to diketonate. Moreover, the #1 and #2 processes have practically the same density difference map. This is related to the mentioned insensitivity of these maps to the phase of combined orbitals. Another couple of states show more complicates aspect of intra-ligand processes.

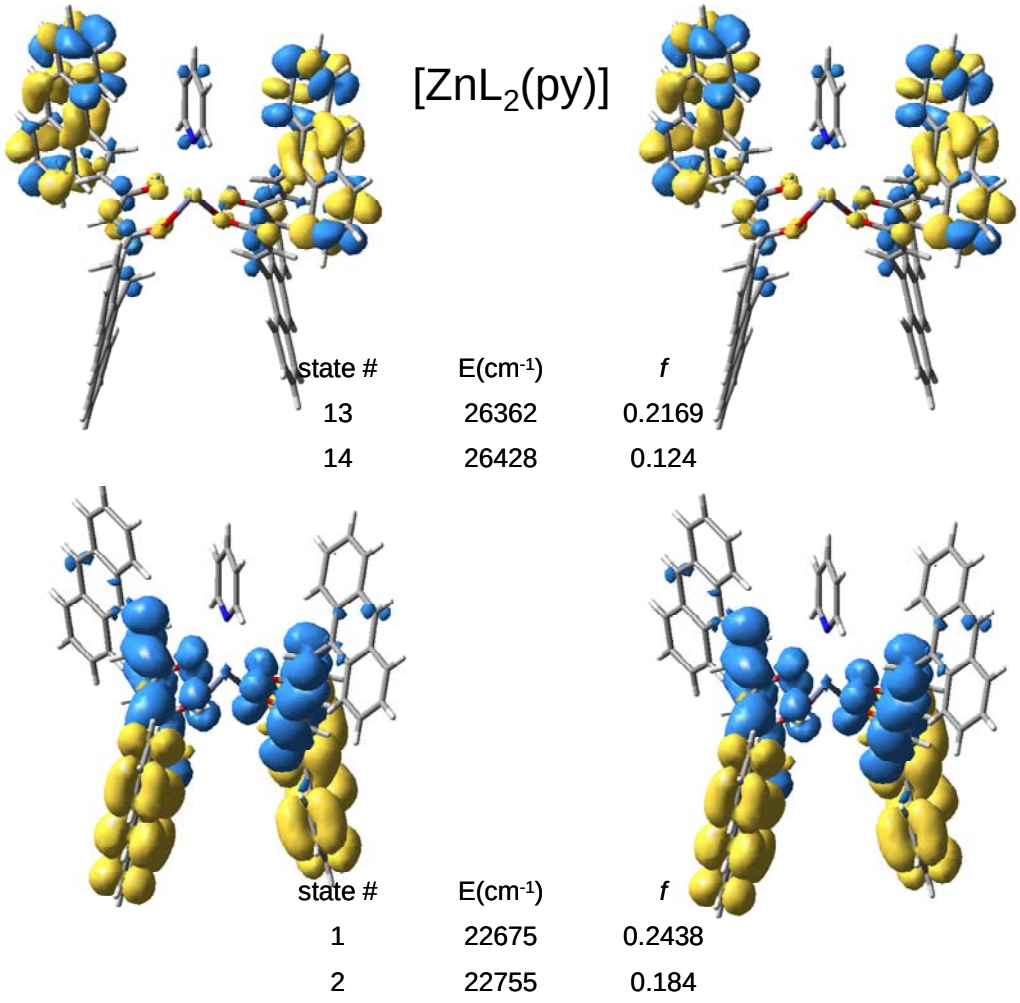

Figure S22.

While a stable and a general feature of the all systems seems to be related, with a transition between anthranyl and diketonate moieties, the higher active bands are sensitive to details of mutual placements of the ligands or with respect of the mutual orientation of the anthracene fragments in the same ligand. The slight differences between the anthracene groups decide which actual one is more active in a given process.